A Fast 3D Interface Simulator for Steamdrives

R.R. Godderij,* Johannes Bruining, and **J. Molenaar,**** Delft U. of Technology

Summary

Here we describe a fast 3D steam drive simulator. We use an interface model, where the single-phase steam zone is separated from the two-phase liquid zone by the steam condensation front (SCF) which constitutes the interface. Steady-state heat balances applied at the interface reduce the steam problem to a problem of gas/oil/water flow. Heat losses are treated by a prescribed conversion of steam to water. The model incorporates gravity, viscous and capillary forces and handles arbitrary permeability distributions and well configurations.

We use a multigrid method to solve the pressure equation. The steam zone development is determined by a probabilistic method, which ensures that instability phenomena are properly treated. The oil/water flow problem in the liquid domain is solved as in conventional reservoir simulators. We validate the model with analytical models.

Example calculations for a thin medium-viscosity oil field show that a transition zone with a reduced oil viscosity just downstream of the SCF has a pronounced stabilizing effect. This, and the global heat loss effects are the reason for the high displacement efficiency of steam drives.

Introduction

Steam drive models with various degrees of sophistication are available for optimal field development and the assessment of economical risks. Fast, simple models solve the heat-balance equation and use *a priori* assumptions on the flow field. Examples are the frontal displacement models[1-3] or the extreme gravity overlay models (a horizontal SCF).[4-6] Van Lookeren[7] was the first who combined a heat balance with mass flow. His description results in a stationary development of an inclined steam condensation front. It is, however, only applicable for favorable (pseudo) mobility ratios. Limitations of simple analytical models, and the ready availability of computers led to the development of thermal reservoir simulators.

Here, we describe a model that incorporates the essential features of the steam drive process but uses some assumptions to lower the computational costs. The main assumption lies in the application of steady-state heat and mass balances over the SCF to reduce the problem to the model equations of gas/water/oil flow. The essential ideas are described extensively in previous references.[8-10] In these papers, we used an effective viscosity in the single-phase liquid zone. Therefore, we could only describe the steam zone expansion and not predict oil and water production. Moreover, due to the vertical equilibrium (VE) assumption, we could not deal with steam underride in a low lying high permeable layer.

In this paper, we present a 3D steam drive model which includes a two-phase liquid zone and allows arbitrary injection/production well configurations. We describe the expansion of the steam zone with a probabilistic method[11-14] to deal with the possible unstable nature of the displacement process. For this, the probabilistic method was extended to 3D.

The main application of the model is to aid in the design and interpretation of steam drive projects. The model can be used: (1) to describe the shape of the steam zone in three dimensions, (2) to predict the time of steam breakthrough, (3) to calculate the cumulative water and oil productions for each well, and (4) to determine the relative importance of features related to the steam drive process such as steam override, viscous fingering, and steam and/or water cresting/coning in fine gridded homogeneous and heterogeneous reservoirs.

Physical Model

Reservoir Geometry. Fig. 1 shows a 3D representation of a tilted rectangular heterogeneous reservoir,with thickness d, width b, and length L. It is bounded by impermeable cap and base rock with constant thermal properties. The reservoir tilt can be described by two angles: (1) the angle between the x axis and the horizontal plane, θ_1, and (2) the angle between the y axis and the horizontal plane, θ_2. The flow domain Ω consists of three zones: (1) a steam zone Ω_s, (2) a liquid zone Ω_l, and (3) an upstream and a downstream transition zone surrounding the steam condensation front Γ_{sl} which separates the steam zone from the liquid zone. Injection and production occur via an arbitrary number of wells, with an arbitrary orientation in the reservoir.

Initial and Boundary Conditions. The reservoir is initially filled with dead oil and irreducible water. Compositional effects can be neglected for heavy oil. We apply no flow boundary conditions to the outer boundaries of the domain Ω except for the part of the cap and base rock where an outward steam flux compensates for 1D conductive heat losses (see Appendix B). The water of condensation moves along with the steam towards the steam condensation front.

Injection and Production. The number, location, orientation, and perforated interval of the injection and production wells is arbitrary. Injection wells are operated at a constant rate $Q_{s,\mathrm{inj}}$, temperature T_s, and steam quality f_s, which is the steam mass fraction of the injected steam-water mixture. Production wells are operated at a constant bottomhole flowing pressure p_w.

The Steam Zone Ω_s. The steam zone has a uniform steam S_s, residual oil S_{ors}, and water saturation S_w, and a constant temperature T_s. We assume that the fluids, i.e., also steam, are incompressible and neglect their thermal expansion. Some water can stay behind in the steam zone, thus reducing the effective steam mobility. We assume that the remainder of the water of condensation, and the injected water (for $f_s<1$) are immediately transported to the steam condensation front where it is redistributed proportional to the total velocities normal to the steam condensation front. Therefore, we only consider one-phase flow of steam and assume that Darcy's law is applicable. We incorporate a capillary pressure term to provide a mechanism that inhibits the steam from flowing from a high to a low permeable zone.[15] We disregard the saturation dependence of the capillary pressure in the single-phase steam zone and obtain

$$P_c^{os}=\sigma_{os}\sqrt{\frac{\phi}{k}}J(S_{ss})=\gamma\sigma_{os}\sqrt{\frac{\phi}{k}}. \quad (1)$$

The constant γ gives the value for the J function at some average saturation S_{ss}. For saturations of 50%, it typically assumes values[16] between 0.3 and 0.7.

---

*Now at Veba Oil Nederland B.V.
**Now at Logica B.V.

This paper (SPE 59269) was revised for publication from paper SPE 38288, prepared for the 1997 SPE Western Regional Meeting held in Long Beach, California, 25–27 June. Original manuscript received for review 10 July 1997. Revised manuscript received 11 January 1999. Manuscript peer approved 9 July 1999.

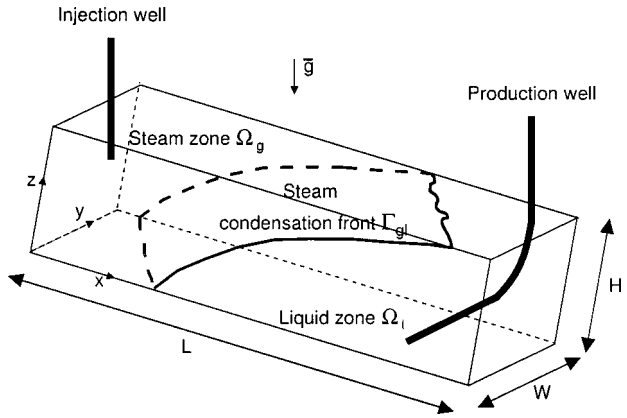

Fig. 1–3D schematic of a tilted reservoir with a steam zone Ω_s, a liquid zone Ω_l, and the steam condensation front Γ_{sl} separating the steam and liquid zone. We included an arbitrary well-layout with a vertical injection and a horizontal production well.

The Transition Zones. Fig. 2 shows the water and steam saturation, and the temperature versus distance in the transition zones. We define an upstream transition zone to incorporate the decrease in the steam saturation from $S_s = 1 - S_{iw} - S_{ors}$ in the steam zone to $S_s = 0$ at the SCF. We describe this by a constant reduced steam mobility in a zone of length δx just upstream of the SCF. We assume that the oil-steam capillary pressure is zero at the steam condensation front because $S_s = 0$.

We define a downstream transition zone to incorporate the decrease in the temperature from the steam temperature T_s at the SCF to the initial reservoir temperature T_r further downstream. The associated increase of the oil viscosity from the low hot oil viscosity to the high cold oil viscosity is modeled by a constant high oil mobility in a zone of length δx just downstream of the SCF.

The Normalization Factor. The condensation of steam at the front results in a discontinous normal component of the total volumetric flow. The ratio of the normal components of the specific discharge leaving the front Q_l^+ and the specific discharge impinging on the front Q_s^- is called the normalization factor[8] m. The superscripts $-$ and $+$ denote the upstream and downstream side of the SCF. A rigorous derivation of the normalization factor is given in Appendix A. It involves the solution of the semisteady-state heat and mass balances over the transition zone, which leads to

$$m = \frac{Q_w^-}{Q_s^-} + \frac{\rho_s}{\rho_w} + \frac{\phi S_s \rho_s \beta}{1 + \phi S_s \rho_s \beta}\left(1 - \frac{\rho_s}{\rho_w}\right). \quad (2)$$

The normalization factor is assumed constant along the steam condensation front. It is a function of time because the heat losses to cap and base rock change the ratio of water and steam impinging on the steam condensation front, i.e., Q_w^-/Q_s^-. The introduction of m allows the coupling of the flow of steam just upstream of the transition region to the flow of oil and water just downstream of the transition region.

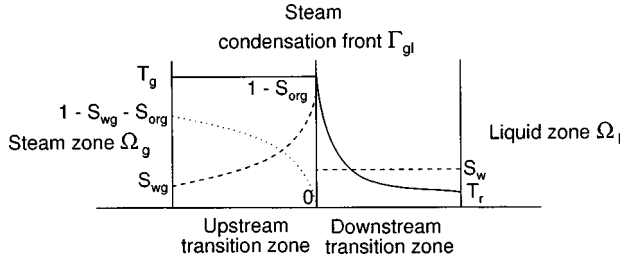

Fig. 2–Schematic diagram of the water saturation (dashed line), the steam saturation (dotted line), and the temperature distribution (solid line) within the upstream and downstream transition region.

The Liquid Zone Ω_l. The liquid zone contains a mixture of oil S_o and water S_w and has a constant temperature T_r, i.e., the initial reservoir temperature. We consider incompressible two-phase flow of oil and water and assume that Darcy's law holds. We use the Brooks–Corey model[17] for the oil and water relative permeabilities and the oil water capillary pressure. They are given by

$$\left.\begin{aligned} k_{ro} &= k'_{ro}(1 - S_{we})^2(1 - S_{we}^{[(2+\eta)/\eta]}) \\ k_{rw} &= k'_{rw} S_{we}^{[(2+3\eta)/\eta]} \\ P_c^{ow} &= \gamma \sigma_{ow} \sqrt{\frac{\phi}{k}}\, 0.5^{(1/\eta)} S_{we}^{(-1/\eta)} \end{aligned}\right\}, \quad (3)$$

where $S_{we} = (S_w - S_{iw})/(1 - S_{iw} - S_{orw})$ and where $k'_{r\alpha}$ are the end-point permeabilities. We have replaced the bubbling pressure P_{cb} in the Brooks–Corey model by $\gamma \sigma_{ow} \sqrt{\phi/k}\, 0.5^{1/\eta}$. This is accomplished by using $J(S_{we} = 0.5) = \gamma$ with $0.3 < \gamma < 0.7$.

Steam Zone Expansion. We use a probabilistic method to determine the steam zone expansion. The method is based on the idea that the velocity at a certain location can be interpreted as the expansion probability at that location. Large velocities have a high expansion probability.

For a detailed description of the probabilistic method, we refer to the articles of King[11-14] whose work is based on a stream function formulation. The probabilistic approach is particularly well suited for unstable displacement processes as the method constantly perturbs the solution.

For unstable displacement processes, each realization has a different displacement profile but a more or less similar recovery and breakthrough time. For stable displacement processes, each realization should lead to essentially the same result as for a deterministic solution. King[13] has shown that the probabilistic method indeed gives similar results as deterministic methods for a variety of stable displacement processes.

Van Batenburg[18] followed King's approach to model 2D underground coal gasification. Frick *et al.*[19] use a 2D pressure formulation instead of a 2D stream function formulation. The advantage of such a pressure formulation is that it can be more easily extended to 3D. Biezen[20,21] successfully applied the combination of the 3D pressure formulation and the probabilistic method to underground coal gasification. This procedure is also used here.

Flow in the Liquid Zone. In the liquid zone, we solve the two-phase flow equation by a conventional finite difference method. Each time step we calculate the specific discharges of water by applying Darcy's equation with upstream weighted values for the mobilities.

At the steam condensation front we use the assumption that the fractional flow of water is determined by the ratio of the volume of water over the total volume of oil and water leaving the steam zone. The volume of water is the total of: (a) coinjected water, (b) water formed by condensation of steam corrected for the water remaining in the steam zone, and (c) the volume of water displaced by steam. The volume of oil equals the volume of oil displaced by steam. This procedure preserves overall mass conservation.

Model Equations

The model equations are summarized in Appendix B. In summary, we have as model equations a total fluid conservation law (Eq. B-7b), in which the discharges are expressed in terms of pressures in Eqs. B-3, B-4, and B-7 for the steam zone, liquid zone and at the SCF, respectively. Injection and production through the wells is prescribed in Eq. B-7b. Boundary conditions are of the no-flow or given flow (Eq. B-8) type. The water saturation changes in the liquid zone are given by the water conservation Eq. B-9; the water discharges are given in Eq. B-10, where

we use Eq. B-11. The discretization of the model equations is given in Appendix C. The steam zone expansion is described by the probabilistic method.[21]

Solution Procedure

The procedure starts with the determination of the phase mobilities and the productivity indexes of the wells. The time discretization, Eq. B-9, is chosen such that the steam zone expands one grid cell per time step. Therefore, the time step is determined by the time required to inject a volume of steam which: (1) heats up a liquid filled grid cell and saturates it with steam, and (2) compensates for heat losses. The time step can be calculated from

$$\Delta t = \frac{h_x h_y h_z}{Q_s^-}\left(\frac{1}{\beta\rho_s} + \phi S_s\right), \tag{4}$$

where the heat factor β and the total discharge Q_s^- are given in Appendix A. We use the old pressure field to determine the flow direction for the upstream weighted mobilities used in Eqs. C-2, C-3, and C-4. We solve Eq. C-1a with a multigrid method, developed by Molenaar,[22,23] to obtain the new pressure field and from it the new generalized volume flux field. Such a multigrid solver is superior to other iterative methods as the amount of computational work is proportional to the number of grid points.

We determine the steam zone expansion for a single time step according to the following procedure: (1) calculate the total flow, mQ_s, from steam locations through all steam faces which are exposed to liquid, (2) draw a single random number,[24] $\mathcal{R}_1$, uniformly distributed between zero and one, (3) repeat the summation over the steam-liquid faces until the value $\mathcal{R}_1 mQ_s$ is reached. At this location a block of liquid is displaced by steam.

The next step is to solve the water conservation Eq. C-5 on $\Omega_l \cup \Gamma_{sl}$. At all block faces between liquid filled blocks, we determine q_w with Eq. C-6 using Eq. C-3. At all block faces between steam and liquid filled blocks, we determine q_w with Eq. C-6. We calculate u_t with Eq. C-4 and $f_{w,\text{int}}$ with Eqs. B-11, B-12, and B-13. The time step defined in Eq. 4 may be too big for a stable solution of Eq. C-5. In that case we take a few consecutive time steps until the sum of the time steps for the water conservation equation equals the time step given by Eq. 4. Finally, we calculate the phase productions with Eq. C-1b. The new saturations are used to calculate the new phase mobilities, etc.

Validation of the Simulator

To validate the 3D simulator, we performed a number of 1D and 2D simulations and compared the results with known analytical solutions and/or experimental results. We use:

The 1D Marx–Langenheim problem to validate the heat transfer mechanisms in our simulator. We find excellent agreement in steam condensation front positions. This shows that the heat balance errors are negligible. As also is expected theoretically indeed the probabilistic approach does conserve energy.

The 1D Buckley–Leverett problem to validate the two-phase flow in the liquid zone. We find excellent agreement of constant state saturations in the downstream liquid zone.

Two 2D pattern drives to validate the treatment of the viscous forces in the areal plain. The simulations are carried out for a pseudo mobility ratio M of 1 and 7.3, respectively, where the pseudo mobility ratio is given by

$$M = \frac{mk_{rs}/\mu_s}{k_{ro}/\mu_o + k_{rw}/\mu_w}. \tag{5}$$

For $M=1$ and for $M=7.3$, we find an areal coverage at breakthrough of 0.72 and 0.54, respectively. This agrees well with the literature data of 0.72 and 0.53, respectively.[25,26]

The inclination of SCF to validate the treatment of viscous and gravity forces in the vertical plain. The simulations are carried out for a reservoir dip of 11°, a gravity number G_x of 4.3 and a pseudo mobility ratio M of 0.25 and 2.5. The dimensionless gravity number is given by

$$G_x = G\sin(\theta_1) = \frac{kk_{rs}\Delta\rho_{ls}db\sin(\theta_1)}{\mu_s Q_s} \tag{6}$$

with $\Delta\rho_{ls} = (\lambda_w\rho_w + \lambda_o\rho_o)/(\lambda_w + \lambda_o) - \rho_s$.

Dietz's theory for oil-water displacement adapted for steam-oil displacement reads

$$\frac{dz}{dx} = \begin{cases} \dfrac{1-M}{G} & \text{for } \theta_1 = 0 \\ \dfrac{G_x + 1 - M}{G_x}\tan(\theta_1) & \text{for } \theta_1 \neq 0 \end{cases}. \tag{7}$$

The displacement is stable for $M \leqslant G_x + 1$. We compare the inclination of the steam condensation front according to Eq. 7 with the simulated shape of the steam condensation front. For $M=0.25$ and $G_x=4.3$, the angle computed with Eq. 7 is 13°. For $M=2.5$ and $G_x=4.3$, we obtain 7°. As expected it takes some time before the steady state angle in the numerical computations has been reached. When the interface is at the middle of the reservoir average agreement between numerical and analytical results is good.

The effect of grid size and the number of realizations to validate numerical convergence. For our base case with a pseudo mobility ratio M of 17.8 and a gravity number G_x of 8.6, we found that a $64\times1\times16$ grid is sufficient. For more adverse mobility ratios ($M \gg 1$) or stronger gravity override conditions ($M \gg G_x + 1$), the required number of grid blocks would increase for an accurate simulation of the steam breakthrough times.

The probabilistic method requires several realizations per case. The required number of realizations[27] is given by $n_0 = (t\hat{s}100/P\mu_0)^2$. This number follows from a Student's t-test with a certain confidence interval for the sweep efficiency at steam breakthrough with P % error. The required number of realizations for a 95% confidence interval for a maximum error of 5% in the recovery at steam breakthrough is less than 5 for all simulations considered in this paper.

Results and Discussions

Scaled model experiments[8] showed much less steam override than one would expect from a viscous force ratio with steam flowing upstream and cold oil flowing downstream. Here, we present some vertical 2D example calculations that explain the observation. We show the effect of: (A) a single-phase liquid region with a constant mobility, (B) a two-phase liquid region, (C) a low steam end-point permeability in the steam zone, (D) a low oil viscosity in the liquid zone, (E) a one grid block wide upstream transition zone with a reduced steam mobility, (F) a one grid block wide downstream transition zone with an enhanced oil mobility, (G) an upstream and downstream transition with a reduced steam and an enhanced oil mobility, respectively.

Tables 1 and 2 define the constant and case specific input parameters. We use the saturated steam-water correlations of Tortike and Farouq Ali.[28] **Table 3** presents the average steam breakthrough times, the recoveries, and total fluid productions at steam breakthrough for 10 realizations per case. Each realization for the 1,024 grid blocks takes approximately 2 min on a HP735 workstation. **Fig. 3** shows the steam zone and the downstream water saturation for 1 realization per case after 0.175 PV of steam injected in cold water equivalents.

For case A, we have a single-phase liquid zone and a single-phase steam zone. The pseudo mobility ratio M of 17.8 and the gravity number G_x of 8.6 lead to an unstable displacement regime because $G_x + 1 - M < 0$.

For case B, we have a two-phase liquid zone. Table 3 and Fig. 3 show that the water in the downstream zone does not delay the steam breakthrough time nor enhance the fluid recoveries compared to case A. The prevailing water saturation just ahead of the SCF is 0.25. The relative permeabilities for oil and water, and the oil and water viscosity lead to an effective pseudo mobility ratio M of 21.1 and a gravity number G_x of 9.3. These values are higher than for case A and cause unstable displacement. The water in the

TABLE 1– MODEL CONSTANTS FOR THE EXAMPLE CALCULATIONS

Property	Symbol	Value	Unit
Length	L	1.736	m
Width	b	0.368	m
Thickness	d	0.08	m
Permeability	k	3,100	μm^2
Effective porosity	ϕS_s	0.342	-
Reservoir dip 1	θ_1	11.0	-
Reservoir dip 2	θ_2	0.0	-
Thermal conductivity	λ_f	0.32	W/(m·K)
Thermal diffusivity	α_f	1.5E−7	m^2/s
Heat capacity of rock	$(\rho c)_m$	2.1E6	J/(kg·K)
Reservoir temperature	T_r	293	K
Steam temperature	T_s	353	K
Injection rate	Q_{inj}	0.833E−6	m^3/s
Steam quality	f_s	1.0	-
Number of grid blocks	$N_x \times N_y \times N_z$	64×1×16	-
Water viscosity	μ_w	1.0E−3	Pa·s
Water density	ρ_w	1,000.0	kg/m^3
Oil density	ρ_0	800.0	kg/m^3
Sorting factor	η	3.0	-
Water end point permeability	k'_{rw}	1.0	-
Oil end point permeability	k'_{ro}	1.0	-
Oil-water interfacial tension	σ_{ow}	0.03	N/m
Oil-steam interfacial tension	σ_{os}	0.03	N/m
Residual oil saturation	S_{ors}	0.05	-
Irreducible water saturation	S_{iw}	0.05	-

downstream zone starts to enhance the downstream mobility for water saturations above 0.28 and leads to stable displacement for water saturations above 0.34.

For case C, we have a ten times lower steam end-point permeability. Table 3 and Fig. 3 show that the reduced steam end-point permeability does not delay the steam breakthrough time nor enhance the fluid recoveries compared to case B. The prevailing water saturation of 0.24 just ahead of the SCF and the reduced steam end-point permeability lead to a pseudo mobility ratio M of 2.2 and a gravity number G_x of 0.9. These conditions are more favorable but still lead to unstable displacement.

For case D, we have a four times lower oil viscosity. Table 3 and Fig. 3 show that the reduced oil viscosity significantly delays the steam breakthrough time and enhances the fluid recoveries. The prevailing water saturation of 0.3 just ahead of the SCF and the reduced oil viscosity lead to a pseudo mobility ratio M of 7.1 and a gravity number G_x of 9.2. This gives indeed a gravity stable displacement process.

For case E, we have a region of one grid block just upstream of the SCF with a ten times lower steam permeability than in the remainder of the steam zone. Table 3 and Fig. 3 show that the upstream transition zone does not significantly delay the steam breakthrough time or enhance the fluid recoveries. The prevailing water saturation of 0.24 just ahead of the SCF and the reduced steam end-point permeability in the upstream transition zone lead to a pseudo mobility ratio M of 2.2 and a gravity number G_x of 0.9. The dimensionless numbers have exactly the same values as for case C and are representative for unstable displacement. The steam breakthrough times and recoveries are also the same as for case C.

TABLE 2– SPECIFIC INPUT PARAMETERS FOR THE EXAMPLE CALCULATIONS

Case	k'_{rs} (−)	μ_0 (Pa·s)	2-ph. Liq. Zone	k'_{rs} in Upstr. Transition Zone	μ_0 in Downstr. Transition Zone
A	1.0	0.070	No	1.0	0.070
B	1.0	0.070	Yes	1.0	0.070
C	0.1	0.070	Yes	0.1	0.070
D	1.0	0.017	Yes	1.0	0.017
E	1.0	0.070	Yes	0.1	0.070
F	1.0	0.070	Yes	1.0	0.017
G	1.0	0.070	Yes	0.1	0.017

TABLE 3– AVERAGE STEAM BREAKTHROUGH TIME, THE AVERAGE OIL RECOVERY AT STEAM BREAKTHROUGH, AND THE AVERAGE TOTAL PRODUCTION AT STEAM BREAKTHROUGH FOR 10 REALIZATIONS OF CASES A–G IN PV

Case	SBT	REC at SBT±Standard Deviation	TOT at SBT
A	0.3124		1.0686
B	0.3246	0.8024±0.009	1.0981
C	0.3269	0.8054±0.009	1.1035
D	0.3764	0.8548±0.008	1.2129
E	0.3251	0.7987±0.009	1.0939
F	0.3773	0.8525±0.014	1.2156
G	0.3678	0.8449±0.011	1.1948

For case F, we have a region of one grid block downstream of the SCF with a four times lower oil viscosity than in the remainder of the liquid zone. Table 3 and Fig. 3 show that the downstream transition zone significantly delays the steam breakthrough time and enhances the fluid recoveries compared to case B. The prevailing water saturation of 0.28 just ahead of the SCF and the reduced oil viscosity in the downstream transition zone lead to a pseudo mobility ratio M of 7.2 and a gravity number G_x of 9.2. The dimensionless numbers have exactly the same values as for case D and are representative for stable displacement. The steam breakthrough times and recoveries are also the same as for case D. The effect of the local mobility ratio on the stability of displacement processes was stressed previously in articles of Hagoort[29] and King.[14]

For case G, we have two regions of one grid block with the properties of case E and case F, respectively. Table 3 and Fig. 3 show that the two transition zones significantly delays the steam breakthrough time and enhance the fluid recoveries. The prevailing water saturation of 0.29 just ahead of the SCF and the two transition zones lead to a pseudo mobility ratio M of 0.7 and a gravity number G_x of 0.9. The dimensionless numbers are representative for stable displacement.

Summarizing it can be said that a higher mobility in the downstream transition zone stabilizes the SCF, i.e., affects the shape of the SCF. The high mobility is caused by heat penetration into the liquid zone. In the interface model, the heat penetration depth needs to be estimated. Usually, the penetration depth is small with respect to the grid size. Hence, also in a reservoir simulator that

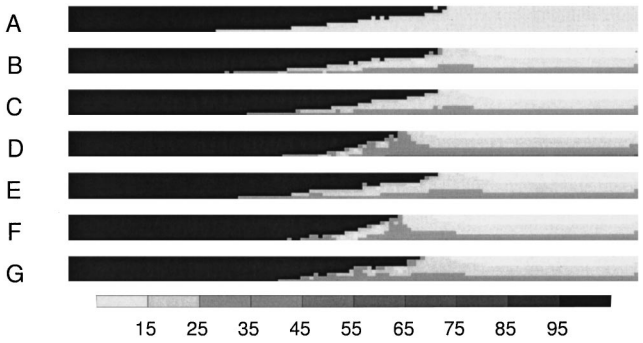

Fig. 3–Steam zone (black) and the water saturation (gray scale) in the downstream zone for one realization per case after 0.175 PV of steam injected in cold water equivalents.

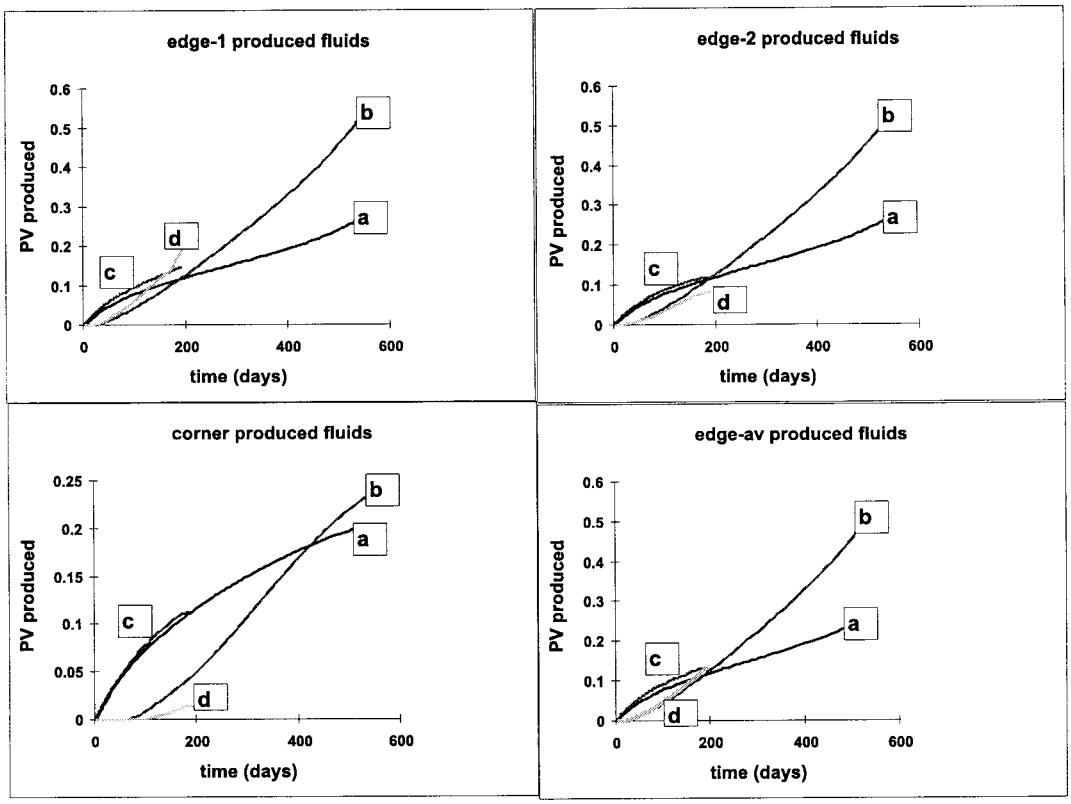

Fig. 4–Comparison between simulation results with STARS and simulation results with the interface simulator. From the top left clockwise edge producer (1), edge producer (2), the average of the edge producers and the corner producer. The curves labeled (a) and (c) show the cumulative oil production obtained with STARS and the interface simulator, respectively. The curves labeled (b) and (d) show the cumulative water production obtained with STARS and the interface simulator.

solves the heat balance equation in the liquid zone it is expected that the viscosity distribution ahead of the SCF is largely dependent on the grid size.

Comparison to the Fourth SPE Comparative Solution Project

We have simulated problem 2A of the fourth SPE comparative solution project (SPE 13510).[30] The reservoir ($100\,m^3 \times 100\,m^3 \times 25\,m^3$) consists of a symmetry element of a nine spot with an injection well at the center, four edge producers, and four corner producers. The reservoir has four layers with permeabilities from top to bottom of 2.0, 0.5, 1.0, and 2.0 Darcy. The porosity is 30%. The injection rate is 300 bbl/day of steam (cold water equivalent) with a steam quality of 70%, independent of the injection pressure. The production pressure is 17 psi and the maximum total production rate is 1,000 bbl/day. The SPE project uses one eighth of the area with one injection well, one edge producer and one corner producer. The reservoir is divided in $9 \times 5 \times 4$ grid blocks. We use one fourth of the reservoir divided in $16 \times 16 \times 4$ grid cells. We also use a constant layer thickness. We run our simulations until steam breakthrough because the interface model assumes residual oil in the steam zone and thus after breakthrough no further oil is produced. Finally, the problem as presented has a significant compressibility effect. As this cannot be approximated by incompressible flow the comparison is poor. Here, we use a much lower (realistic) rock compressibility of $5.0E-6(psi^{-1})$ as opposed to the rock compressibility $5.0E-4(psi^{-1})$ used in the program. The insensitivity to the steam compressibility can be understood as the steam zone expansion is determined by the heat balance equation. Our comparison is with the STARS[31] simulation output. We redid the simulations with STARS such that the comparison is made for exactly the same input data, including the grid cell division.

The results are shown in **Fig. 4**. The figure compares cumulative oil and water production of the STARS simulator with the Interface Simulator. Clockwise it shows the results for edge producer (1), edge producer (2), the average of the edge producers and for the corner producer. In spite of symmetry, the interface simulator gives different results for the two individual edge producers thanks to the probabilistic method to compute the time evolution. Therefore, we use the average cumulative production of the edge producers for the comparison. The average production shows reasonable agreement between the simulators until steam breakthrough. There is a significant difference in the simulation results of the cumulative water production for the corner producer, but in view of the difference in scale the water production is still small. The steam breakthrough occurs earlier in our model due to the unstable nature of the displacement process. Unstable displacement (i.e., where distinctive unstable fingering should occur) cannot be straightforwardly modeled by a finite difference or finite element reservoir simulator. The probabilistic method used here[11-14] is a procedure to handle unstable displacement more realistically, but it is still not perfect (see also Ref. 32). Indeed the unstable nature of the displacement is underestimated also in our model due to the large gridblock size. Still, the agreement between the simulators until breakthrough for edge and corner producers is good, except for the small water production of the corner producer. As to calculation times they are comparable. This was due in part to the fact that modeling the unstable displacement process led to the use of extremely small timesteps by our model for solving Eqs. C-5 to C-6, i.e., to distribute the water in the liquid zone. In summary, the agreement with the SPE project example 2A is, however, good.

Conclusions

- We have developed a computationally fast 3D steam drive simulator based on an interface model.
- The model is suited for high resolution studies of the steam drive process and its important physical mechanisms.

- The simulations have demonstrated that a two-phase liquid zone stabilizes or destabilizes the displacement depending on whether water increases or decreases the total downstream mobility.
- The simulations have demonstrated the stabilizing effect of a reduced oil viscosity in the downstream transition zone.
- The simulations have demonstrated that the stability of the steam condensation front is determined by the local and not the global values of the pseudo mobility ratio and the gravity number.
- The model accurately describes the shape of the steam zone in unstable conditions.
- The application of our model lies in predicting the time of steam breakthrough. In our simulator, production stops after steam breakthrough due to the assumption that we have residual oil in the steam zone.
- There is good agreement between production profiles from a commercial simulator output and from our simulation for input conditions of problem 2A defined in the fourth comparative program. However, we use much lower (realistic) values for the compressibility.

Nomenclature

Greek

α_f = thermal diffusivity, m^2/s
β = heat factor, m^3/kg
χ = proportionality constant
$\delta(r)$ = distribution function, $1/m^3$
$\Delta\rho_{ls}$ = liquid-steam density difference, kg/m^3
ΔT = temperature difference, K
ΔV_s = steam zone expansion, m^3
ϕ = porosity
γ = constant in Leverett-*J* function
η = constant in Brooks–Corey model
λ_f = thermal conductivity, $J(s\,m\cdot K)$
λ = mobility, $m^2/(Pa\cdot s)$
μ = dynamic viscosity, $(Pa\cdot s)$
μ_0 = average sweep efficiency
θ = rotation angle, degrees
ρ = density, kg/m^3
σ = interfacial tension, $Pa\cdot m$
τ = time of first exposure to steam, s
Ω = domain
Γ_{sl} = steam condensation front

Latin

A = area, m^2
b = width, m
c = specific heat, $J/(kg\cdot K)$
C_A = Dietz shape factor
$\overline{e_\zeta}$ = unit vector
f_s = steam quality
f = fractional flow
g = acceleration due to gravity, m/s^2
G = gravity number
$G(t,\tau)$ = steam condensation rate, m/s
h = grid spacing, m
d = thickness, m
$I_{i,j,k}$ = indicator function
$J(S)$ = Leverett-*J* function
k = permeability, m^2
k' = end-point permeability
L = length, m
L_v = heat of vaporization, J/kg
m = normalization factor
M = pseudo mobility ratio
n = number of wells
n_0 = number of samples
N = number of grid blocks
p = pressure, Pa
P = tolerance
P_c = capillary pressure, Pa
P_{cb} = capillary entrance pressure, Pa
q = specific discharge, m/s
$\mathbf{q}$ = specific discharge vector, m/s
Q = flow rate, m^3/s
r = radius, m
$\mathcal{R}_1$ = random number
$\hat{s}$ = the estimated standard deviation
s = skin factor
S = saturation
t = Student's *t*-test
t = time, s
T = temperature, K
u = generalized volume flux, m/s
$\mathbf{u}$ = generalized volume flux vector, m/s
v_f = front velocity, m/s
V = volume, m^3
x,y,z = space coordinates, m

Superscripts

$+$ = upstream
$-$ = downstream

Subscripts

α, = phase
dt = downstream transition zone
i = index
inj = injected
int = interface
l = liquid
o = oil
os = oil steam
ow = oil water
p = produced
r = relative
s = steam
t = total
ut = upstream transition zone
w = water
x,y,z = x,y,z direction

Acknowledgments

We thank the Delft U. of Technology and the Nederlandse Aardolie Maatschappij (Shell and EXXON) for supporting this project. We thank O.H. Barzandji for his help with the STARS simulator.

References

1. Marx, J.W. and Langenheim, R.H.: ''Reservoir Heating by Hot Fluid Injection,'' *Trans.*, AIME (1959) **216**, 312.
2. Mandl, G.W. and Volek, C.W.: ''Heat and Mass Transport in Steamdrive Processes,'' *SPEJ* (March 1969) 59; *Trans.*, AIME, **246**.
3. Myhill, N.A. and Stegemeier, G.L.: ''Steamdrive Correlation and Prediction,'' *JPT* (February 1978) 173.
4. Neuman, C.H.: ''A Gravity Override Model of Steamdrive,'' *JPT* (January 1985) 163.
5. Vogel, J.V.: ''Simplified Calculations for Steamfloods,'' *JPT* (July 1984) 1127.
6. Miller, M.A. and Leung, W.K.: ''A Simple Gravity-Override Model of Steamdrive,'' paper SPE 14241 presented at the 1985 SPE Annual Technical Conference and Exhibition, Las Vegas, Nevada, 22–25 September.
7. van Lookeren, J.: ''Calculation Methods for Linear and Radial Steam Flow in Oil Reservoirs,'' *JPT* (June 1983) 427.
8. Palmgren, C.T.S.: ''Oil Recovery by Steamdrive, an Interface Approach,'' PhD dissertation, Delft U. of Technology, Delft, The Netherlands (October 1992).
9. Palmgren, C.T.S. and Bruining, J.: ''An Interface Model To Predict Vertical Sweep During Steamdrive,'' paper SPE 24077 presented at the 1992 SPE Western Regional Meeting, Bakersfield, California, 30 March–1 April.

10. Godderij, R.R. and Bruining, J.: ''A New Model To Predict Steam Override and Viscous Fingering in Heterogeneous Oil Reservoirs,'' paper SPE 29661 presented at the 1992 SPE Western Regional Meeting, Bakersfield, California, 8–10 March.
11. King, M.J. and Scher, H.: ''Probabilistic Stability Analysis of Multiphase Flow in Porous Media,'' paper SPE 14366 presented at the 1985 SPE Annual Technical Conference and Exhibition, Las Vegas, Nevada, 22–25 September.
12. King, M.J.: ''Probability Approach to Multiphase and Multicomponent Flow in Porous Media,'' *Phys. Rev. A* (1987) **35**(2), 929.
13. King, M.J.: ''Viscous Fingering and Probabilistic Simulation,'' *Numerical Simulation in Oil Recovery*, M.F. Wheeler (ed.), Springer, Berlin (1988) **11**, 161–76.
14. King, M.J. and Dunayevsky, V.A.: ''Why Waterflood Works: A Linearized Stability Analysis,'' paper SPE 19648 presented at the 1989 SPE Annual Technical Conference and Exhibition, San Antonio, Texas, October.
15. Godderij, R.R.G.G. *et al.*: ''An Investigation of the Vertical Sweep Efficiency of Steam Drive in a Layered Reservoir,'' *New Developments in Improved Oil Recovery*, H.J. de Haan (ed.), special publication, Geological Soc., London (1995) 261–273.
16. Dullien, F.A.L.: *Porous Media, Fluid Transport and Pore Structure*, Academic Press, New York City (1989).
17. Brooks, R. and Corey, A.: ''Hydraulic Properties of Porous Media,'' Technical report, Colorado State U. (1964).
18. Van Batenburg, D.W.: ''Heat and Mass Transfer During Underground Gasification of Thin Deep Coal Seams,'' PhD dissertation, Delft U. of Technology, Delft, The Netherlands (December 1992).
19. Frick, T.P. and Zolotukhin, A.B.: ''Field-Scale Stochastic Simulation of IOR Processes,'' *Proc.*, Seventh European IOR Symposium, Moscow (October 1993).
20. Biezen, E.N.J., Bruining, J., and Molenaar, J.: ''An Integrated Model for Underground Coal Gasification,'' paper SPE 30790 presented at the 1995 SPE Annual Technical Conference and Exhibition, Dallas, 22–25 October.
21. Biezen, E.N.J.: ''Modelling Underground Coal Gasification,'' PhD dissertation, Delft U. of Technology, Delft, The Netherlands (April 1996).
22. Molenaar, J.: ''A Simple and Efficient Multigrid Method for Interface Problems,'' *Computational Methods in Water Resources X*, A. Peters (ed.), Kluwer Academic, Dordrecht (1994) 1425–1431.
23. Molenaar, J.: ''A Simple Multigrid Method for 3D Interface Problems,'' *Comput. Math. Appl.* (1996) **31**, 25.
24. Press, W.H. *et al.*: *Numerical Recipes in C*, Cambridge U. Press, Cambridge (1988).
25. Muskat, M.: *The Flow of Homogeneous Fluids Through Porous Media*, McGraw–Hill, New York City (1937).
26. Craig, F.F. Jr., Geffen, T.M., and Morse, R.A.: ''Oil Recovery Performance of Pattern Gas or Water Injection Operations From Model Tests,'' *Trans.*, AIME (1955) **204**, 7.
27. Jensen, J.L., Lake, L.W., and Corbett, P.W.M.: *Statistics for Petroleum Engineers and Geoscientists*, Prentice–Hall, Upper Saddle River, New Jersey (1997).
28. Tortike, W.S. and Farouq Ali, S.M.: ''Saturated-Steam-Property Functional Correlations for Fully Implicit Thermal Reservoir Simulation,'' *SPERE* (November 1989) 471; *Trans.*, AIME, **287**.
29. Hagoort, J.: ''Displacement Stability of Waterdrives in Water-Wet Connate-Water-Bearing Reservoirs,'' *SPEJ* (February 1974) 63; *Trans.*, AIME, **257**.
30. Aziz, K. and Ramesh, B: ''Fourth SPE Comparative Project: A Comparison of Steam-Injection Simulators,'' *JPT* (December 1987) 1576.
31. ''Stars User's Manual, Version 98,'' Technical report, Computer Modelling Group (March 1998).
32. King, M.J. and Datta Gupta, A.: ''Streamline Simulation: A Current Perspective,'' *In Situ* (1998) **22**(1), 91.
33. Dietz, D.N.: ''Determination of Average Reservoir Pressure From Buildup Surveys,'' *JPT* (August 1965) 955; *Trans.*, AIME, **234**.

Appendix A—The Normalization Factor

The condensation of steam at the front results in a discontinuous normal component of the total flow at the front. We use a semisteady-state approach to determine the ratio of the normal components, denoted *m*, between the discharge leaving the steam condensation front Q_1 and the discharge impinging on this moving front Q_s:

$$Q_1 = Q_o + Q_w = m Q_s . \tag{A-1}$$

The velocity of the steam condensation front v_f is given by a semisteady-state heat balance applied over the steady-state transition zone

$$v_f A = \frac{\beta \rho_s Q_s}{1+\beta \rho_s \phi S_s}, \tag{A-2}$$

where

$$\beta = \frac{[1+Q_w^- \rho_w / Q_s^- \rho_s] c_w \Delta T + L_v}{(\rho c)_m \Delta T}. \tag{A-3}$$

The semisteady-state mass balances for oil and water over the semisteady-state transition zone read

$$[Q_w - \phi S_w v_f A]^+ = [Q_w - \phi S_w v_f A]^- + \frac{\rho_s}{\rho_w}[Q_s - \phi S_s v_f A]^-,$$
$$[Q_o - \phi S_o v_f A]^+ = [Q_o - \phi S_o v_f A]^-, \tag{A-4}$$

where superscript $-$ and $+$ denote the upstream steam zone and the downstream liquid zone, respectively. The mass balance equations can be combined and written as

$$Q_1 = Q_w^- + \frac{\rho_s}{\rho_w} Q_s^- + \phi S_s v_f A \left(1 - \frac{\rho_s}{\rho_w}\right). \tag{A-5}$$

Substitution of Eq. A-3 in Eq. A-5 and dividing the last by Q_s^- gives Eq. 2 for *m* in which the volume rates of steam Q_s^- and water Q_w^- at the SCF are given by

$$Q_s^- = \sum_{i=1}^{n_{\text{inj}}} Q_{s,\text{inj},i} - \frac{h_x h_y}{\Delta t} \sum_i^{i\,\max} \sum_j^{j\,\max} \int_t^{t+\Delta t} [G(t, \tau_{i,j,k=1}) + G(t, \tau_{i,j,k=k\,\max})]\,dt, \tag{A-6}$$

$$Q_w^- = \sum_{i=1}^{n_p} Q_{w,\text{inj},i} + \frac{h_x h_y}{\Delta t} \frac{\rho_s}{\rho_w} \sum_i^{i\,\max} \sum_j^{j\,\max} \int_t^{t+\Delta t} [G(t, \tau_{i,j,k=1}) + G(t, \tau_{i,j,k=k\,\max})]\,dt. \tag{A-7}$$

Appendix B—Model Equations

Generalized Volume Flux Vector. Here, we define a generalized volume flux vector $\mathbf{u}_t$ of which the normal component is continuous at the steam condensation front

$$\mathbf{u}_t = \chi \mathbf{q}_t \begin{cases} \chi = m \quad \text{and} \quad \mathbf{q}_t = \mathbf{q}_s & \text{in } \Omega_s \\ \chi = 1 \quad \text{and} \quad \mathbf{q}_t = \mathbf{q}_o + \mathbf{q}_w & \text{in } \Omega_l \end{cases}, \tag{B-1}$$

where *m* is the velocity normalization factor defined in Eq. 2 and $\mathbf{q}_t$ is the specific discharge of steam in Ω_s, and oil and water in Ω_l, respectively. We use Darcy's equation to describe the specific discharge of the different phases

$$\mathbf{q}_\alpha = -\lambda_\alpha (\text{grad}\, p_\alpha - \rho_\alpha g \overline{e_\zeta}), \tag{B-2}$$

where α denotes the phase (steam, oil, or water) and λ_α is the mobility of phase α. It is convenient to express the phase pressures, p_α, in terms of the oil pressure. In the steam zone we use an oil-steam capillary pressure according to Eq. 1 to obtain

$$\mathbf{u}_t = -m\lambda_s (\text{grad}\, p_o - \rho_s g \overline{e_\zeta} + \text{grad}\, P_c^{os}) \quad \text{in } \Omega_s . \tag{B-3}$$

In the liquid zone we use saturation dependent oil-water relative permeabilities and an oil-water capillary pressure according to Eq. 3 to obtain

$$\mathbf{u}_t = -(\lambda_w + \lambda_o)\text{grad}\, p_o + (\lambda_w \rho_w + \lambda_o \rho_o) g \overline{e_\zeta} + \lambda_w \,\text{grad}\, P_c^{ow} \quad \text{in } \Omega_l . \tag{B-4}$$

In the upstream transition zone, we use Eq. B-3 with an average steam mobility. In the downstream transition zone, we use Eq. B-4 with an average oil mobility and an oil-water capillary pressure gradient of zero. At the steam condensation front, Γ_{sl}, $\mathbf{u}_{tn}^+ = \mathbf{u}_{tn}^-$ and $p_o^+ = p_o^-$, where $+$ denotes the upstream transition zone and $-$ denotes the downstream transition zone. We use

$$\mathbf{u}_t = -m\lambda_s(\text{grad}\, p_o^+ - \rho_s g\overline{e_\zeta} + \text{grad}\, P_c^{os^+}) \quad \text{in } \Omega_{ut}, \tag{B-5}$$

$$\mathbf{u}_t = -(\lambda_w+\lambda_o)\text{grad}\, p_o^- + (\lambda_w\rho_w+\lambda_o\rho_o)g\overline{e_\zeta} \quad \text{in } \Omega_{dt} \tag{B-6}$$

to eliminate $p_o^+ = p_o^-$ at Γ_{sl} and obtain

$$\mathbf{u}_t = -\frac{2m\lambda_s^+(\lambda_w^-+\lambda_o^-)}{m\lambda_s^+ + \lambda_w^- + \lambda_o^-}(\text{grad}\, p_o + \text{grad}\, P_c^{os^+}) + \frac{m\lambda_s^+((\rho_s+\rho_w)\lambda_w^- + (\rho_s+\rho_o)\lambda_o^-)}{m\lambda_s^+ + \lambda_w^- + \lambda_o^-} g\overline{e_\zeta}. \tag{B-7a}$$

The stationary conservation law for incompressible flow in the whole domain Ω reads

$$\text{div}\, \mathbf{u}_t = -\sum_{i=1}^{n_{\text{inj}}} mQ_{s,\text{inj},i} + Q_{s,\text{inj},i}\delta(\mathbf{r}-\mathbf{r}_{w,i}) - \sum_{i=1}^{n_p} (Q_{w,p,i} + Q_{o,p,i} + mQ_{s,p,i})\delta(\mathbf{r}-\mathbf{r}_{w,t}), \tag{B-7b}$$

where n_{inj} is the number of injection wells, n_p is the number of production wells, and $\delta(\mathbf{r})$ is the Dirac-delta function which represents a point source/sink. A well is modeled by a series of point sources or sinks on a line. We take $Q_{s,\text{inj}} < 0$ (injection well) and $Q_{o,p}, Q_{w,p}, Q_{s,p} > 0$ (production well).

Substitution of Eqs. B-3, B-4, and B-7 in Eq. B-8 allows to solve the pressure equation for the whole domain Ω for which we define the following initial and boundary conditions.

Initial and Boundary Conditions. The initial saturation distribution is taken $S_w = S_{iw}$ and $S_o = 1.0 - S_{iw}$. We distinguish two boundary conditions: (1) the area of the cap and base rock that is in contact with the steam zone where the heat losses prescribe an outward steam flux

$$u_t = G(t,\tau) = \frac{\lambda_f \Delta T}{\rho_s L_v \sqrt{\pi\alpha_f(t-\tau)}}, \tag{B-8}$$

and (2) the remaining part of the outer boundaries of the domain Ω, which are no flow boundaries, hence $u_t = 0$. The operating conditions for the wells are a constant injection rate for the injection wells and a constant bottomhole flowing pressure for the production wells.

Steam Zone Expansion. We calculate the pressure field and determine the flow field $\mathbf{u}_t$ at the interface Γ_{sl} by the application of Eq. B-7. We determine the location where the steam zone expands with a probabilistic method. The local expansion probability is given by the ratio of the local front velocity over the total front velocity.

Flow in the Liquid Zone. In the liquid zone Ω_l, we solve the water conservation equation, which reads

$$\phi\frac{\partial S_w}{\partial t} + \text{div}\, \mathbf{q}_w = -\sum_{i=1}^{n_p} Q_{w,p,i}\delta(\mathbf{r}-\mathbf{r}_{w,i}), \tag{B-9}$$

where the generalized water discharge, $\mathbf{q}_w$, is given by

$$\mathbf{q}_w = \begin{cases} f_w\mathbf{u}_t + \Lambda\Delta\rho_{wo}g\overline{e_\zeta} + \Lambda\, \textbf{grad}\, P_c^{ow} & \text{in } \Omega_l \\ f_{w,\text{int}}\mathbf{u}_t & \text{at } \Gamma_{sl} \end{cases} \tag{B-10}$$

with $\Delta\rho_{wo} = \rho_w - \rho_o$ and $f_w = \lambda_w/(\lambda_w+\lambda_o)$ and $\Lambda = \lambda_w\lambda_o/(\lambda_w+\lambda_o)$. The fractional flow of water at the steam condensation front $f_{w,\text{int}}$ is given by the ratio of the volume of water over the total volume of oil and water flowing across the steam condensation front

$$f_{w,\text{int}} = \frac{V_{w,\text{int}}}{V_{w,\text{int}} + V_{o,\text{int}}}, \tag{B-11}$$

where $V_{w,\text{int}}$ and $V_{o,\text{int}}$ are given by

$$V_{w,\text{int}} = \phi\Delta V_s(S_w - S_{iw}) - \frac{\rho_s}{\rho_w}\phi\Delta V_s S_s + \sum_{i=1}^{n_{\text{inj}}}\int\left(\frac{\rho_s}{\rho_w}Q_{s,\text{inj},i} + Q_{w,\text{inj},i}\right)dt, \tag{B-12}$$

$$V_{o,\text{int}} = \phi\Delta V_s(1 - S_w - S_{ors}). \tag{B-13}$$

The first terms on the right-hand side of Eqs. B-12 and B-13 represent the volume of water and oil displaced by the expansion of the steam zone by an amount ΔV_s. The second term on the right-hand side of Eq. B-12 represents the volume of steam that saturates the expanded steam zone (converted to a volume of water). The third term gives the total volume of water and steam (converted to a volume of water) injected through the injection wells over a certain time period.

Appendix C—Numerical Model

To obtain an approximate solution of the partial differential Eqs. B-8 and B-9, we define a regular Cartesian $N_x \times N_y \times N_z$ grid system on which we discretize the equations in space and time. The grid cell volume is given by $h_x h_y h_z$, where $h_x = L/N_x$, $h_y = b/N_y$, and $h_z = d/N_z$.

We use a cell-centered implicit pressure, explicit saturation finite-difference scheme with the oil pressure p_o and the water saturation S_w as the independent variables. By cell-centered we mean that the pressure, saturation, and the mobility, are defined in the center of the cell while the velocities are defined on the cell faces. All blocks have their own permeability k. We use upstream weighted mobilities and a harmonic average for the absolute permeability.

Pressure Equation. Integration of the pressure Eq. B-8 over the control volume $h_x h_y h_z$ in the domain Ω yields

$$h_y h_z(u_{t_{i+1/2,j,k}} - u_{t_{i-1/2,j,k}}) + h_x h_z(u_{t_{i,j+1/2,k}} - u_{t_{i,j-1/2,k}}) + h_x h_y(u_{t_{i,j,k+1/2}} - u_{t_{i,j,k-1/2}}) = -I_{i,j,k}(Q_{\text{inj}} + Q_p), \tag{C-1a}$$

where $-(Q_{\text{inj}} + Q_p) = -(mQ_{s,\text{inj}} + Q_{w,\text{inj}} + mQ_{s,p} + Q_{w,p} + Q_{o,p})$ is the inflow volume into cell i,j,k, and $I_{i,j,k}$, an indicator function which is one if a well is defined in the gridcell and zero otherwise. The phase production rates $Q_{\alpha p}$ are given by

$$Q_{\alpha p} = \frac{kk_{r\alpha}}{\mu_\alpha}\left(\frac{2\pi h}{\ln(r_e/r_w) - 1/2 + s}\right)(p_{i,j,k} - p_w). \tag{C-1b}$$

The radius r_e of the drainage area is given by $r_e = 2\sqrt{A/(1.781C_A)}$, where C_A is the Dietz shape factor.[33] The discretized versions of the generalized volume fluxes defined by Eqs. B-3, B-4, and B-7 read for the x direction, i.e., $u_{t_{i+1/2,j,k}} = u_{t_{i+1/2}}$:

$$u_{t_{i+1/2}} = -m\lambda_{s_{i+1/2}}\left[\left(\frac{p_{i+1} - p_i}{h_x}\right) - \rho_s g_x + \left(\frac{P_{c_i}^{os} - P_{c_{i+1}}^{os}}{h_x}\right)\right] \quad \text{in } \Omega_s, \tag{C-2}$$

$$u_{t_{i+1/2}} = -(\lambda_{w_{i+1/2}} + \lambda_{o_{i+1/2}})\left(\frac{p_{i+1} - p_i}{h_x}\right) + (\lambda_{w_{i+1/2}}\rho_w + \lambda_{o_{i+1/2}}\rho_o)g_x + \lambda_{w_{i+1/2}}\left(\frac{P_{c_{i+1}}^{ow} - P_{c_i}^{ow}}{h_x}\right) \quad \text{in } \Omega_l, \tag{C-3}$$

$$u_{t_{i+1/2}} = -\frac{2m\lambda_{s_i}(\lambda_{w_{i+1}} + \lambda_{o_{i+1}})}{m\lambda_{s_i} + \lambda_{w_{i+1}} + \lambda_{o_{i+1}}}\left[\left(\frac{p_{i+1} - p_i}{h_x}\right) + \left(\frac{P_{c_i}^{os}}{h_x}\right)\right] + m\lambda_{s_i}g_x\left[\frac{\lambda_{w_{i+1}}(\rho_w+\rho_s) + \lambda_{o_{i+1}}(\rho_o+\rho_s)}{m\lambda_{s_i} + \lambda_{w_{i+1}} + \lambda_{o_{i+1}}}\right] \quad \text{at } \Gamma_{sl}. \tag{C-4}$$

We omit the *j,k* subscript for convenience. Similar expressions can be given for the *y* and *z* direction.

Water Conservation Equation. Integration of the water conservation Eq. B-9 over the control volume $h_x h_y h_z$ in the domain $\Omega_l \cup \Gamma_{sl}$ yields

$$h_y h_z (q_{w_{i+1/2,j,k}} - q_{w_{i-1/2,j,k}}) + h_x h_z (q_{w_{i,j+1/2,k}} - q_{w_{i,j-1/2,k}}) + h_x h_y (q_{w_{i,j,k+1/2}} - q_{w_{i,j,k-1/2}}) + \phi \frac{\Delta S_w}{\Delta t} h_x h_y h_z = -I_{i,j,k} Q_{w,p}, \quad \text{(C-5)}$$

where $-Q_{w,p}$ is the inflow volume into cell *i,j,k* and $I_{i,j,k}$ is an indicator function which is one if a well is defined in the gridcell and zero otherwise. Eq. C-5 allows the explicit calculation of the new saturations at the new time. The discretized version of the generalized water volume flux defined in Eq. B-10 is for the *x* direction, i.e., $q_{w_{i+1/2,j,k}} = q_{w_{i+1/2}}$, given by

$$q_{w_{i+1/2}} = f_{w_{i+1/2}} u_{t_{i+1/2}} + \Lambda_{i+1/2} \Delta \rho_{wo} g_x + \Lambda_{i+1/2} \times \left(\frac{P^{ow}_{c_{i+1}} - P^{ow}_{c_i}}{h_x} \right) \quad \text{in } \Omega_l, \quad \text{(C-6)}$$

$$q_{w_{i+1/2}} = f_{w,\text{int}} u_{t_{i+1/2}} \quad \text{at } \Gamma_{sl}.$$

We omit the *j,k* subscript for convenience. Similar expressions can be given for the *y* and *z* direction.

SI Metric Conversion Factors

bbl/day	×	1.84	E−06	= m^3/s
Btu/(ft-hr-F°)	×	1.729 58	E00	= W/(m·K)
Btu/(lbm-F°)	×	4.184*	E00	= kJ/(kg·K)
cP	×	1.0*	E−03	= Pa·s
Darcy	×	0.987	E−12	= m^2
dynes/cm	×	1.0*	E00	= mN/m
ft	×	3.048*	E−01	= m
lbm/ft^3	×	1.601 846	E01	= kg/m^3

*Conversion factors are exact. **SPEJ**

Raymond Godderij is a reservoir engineer with Veba Oil Nederland B.V. He previously was with Shell Research. A specialist in reservoir simulation, his main research interest is validation and building of simulators for complex oil-recovery methods and well configurations. Godderij holds a PhD degree from Delft U. of Technology. **Johannes Bruining** is Associate Professor of Reservoir Engineering at Delft U. of Technology in The Netherlands. e-mail: j.bruining@ta.tudelft.nl. He previously was a visiting professor in the Dept. of Petroleum and Geosystems Engineering at the U. of Texas, Austin. He is a specialist in thermal-recovery techniques and multiphase flow in porous media with particular interest in development of dedicated models for complex flow problems in porous media and their validation by laboratory experimentation. Bruining holds a PhD degree in physical chemistry from the U. of Amsterdam. He is a member of the Editorial Review Committee. **Hans Molenaar** currently works with Logica. He is an expert in numerical reservoir simulation with special interest in multigrad methods for reservoir simulation. Molenaar holds a PhD degree from the U. of Amsterdam.